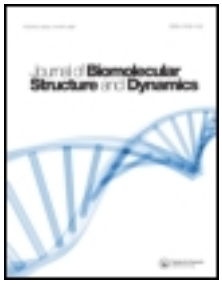

Journal of Biomolecular Structure and Dynamics
Publication details, including instructions for authors and subscription information:
http://www.tandfonline.com/loi/tbsd20

Structural and functional insights into the anti-BACE1 Fab fragment that recognizes the BACE1 exosite

Lucas Joel Gutiérrez [a b], Sebastián Antonio Andujar [a b], Ricardo Daniel Enriz [b c] & Héctor Armando Baldoni [a d]

[a] Área de Química General e Inorgánica, Universidad Nacional de San Luis (UNSL), Chacabuco 917, San Luis, D5700BWS, Argentina

[b] Instituto Multidisciplinario de Investigaciones Biológicas de San Luis (UNSL), CONICET, Ejército de Los Andes 950, San Luis, D5700HHW, Argentina

[c] Cátedra de Química Medicinal, Universidad Nacional de San Luis (UNSL), Chacabuco 917, San Luis, D5700BWS, Argentina

[d] Instituto de Matemática Aplicada San Luis (UNSL, CONICET), Ejército de Los Andes 950, San Luis, D5700HHW, Argentina

Published online: 24 Jul 2013.

To cite this article: Lucas Joel Gutiérrez, Sebastián Antonio Andujar, Ricardo Daniel Enriz & Héctor Armando Baldoni, Journal of Biomolecular Structure and Dynamics (2013): Structural and functional insights into the anti-BACE1 Fab fragment that recognizes the BACE1 exosite, Journal of Biomolecular Structure and Dynamics, DOI: 10.1080/07391102.2013.821024

To link to this article: http://dx.doi.org/10.1080/07391102.2013.821024

Journal of Biomolecular Structure and Dynamics, 2013
http://dx.doi.org/10.1080/07391102.2013.821024

Structural and functional insights into the anti-BACE1 Fab fragment that recognizes the BACE1 exosite

Lucas Joel Gutiérrez[a,b], Sebastián Antonio Andujar[a,b], Ricardo Daniel Enriz[b,c] and Héctor Armando Baldoni[a,d]*

[a]*Área de Química General e Inorgánica, Universidad Nacional de San Luis (UNSL), Chacabuco 917, San Luis D5700BWS, Argentina;* [b]*Instituto Multidisciplinario de Investigaciones Biológicas de San Luis (UNSL), CONICET, Ejército de Los Andes 950, San Luis D5700HHW, Argentina;* [c]*Cátedra de Química Medicinal, Universidad Nacional de San Luis (UNSL), Chacabuco 917, San Luis D5700BWS, Argentina;* [d]*Instituto de Matemática Aplicada San Luis (UNSL, CONICET), Ejército de Los Andes 950, San Luis D5700HHW, Argentina*

Communicated by Ramaswamy H. Sarma

(*Received 18 February 2013; final version received 26 June 2013*)

A molecular modeling study giving structural, functional, and mutagenesis insights into the anti-BACE1 Fab fragment that recognizes the BACE1 exosite is reported. Our results allow extending experimental data resulting from X-ray diffraction experiments in order to examine unknown aspects for the Fab-BACE1 recognition and its binding mode. Thus, the study performed here allows extending the inherently static nature of crystallographic structures in order to gain a deeper understanding of the structural and dynamical basis at the atomic level. The characteristics and strength of the interatomic interactions involved in the immune complex formation are exhaustively analyzed. The results might explain how the anti-BACE1 Fab fragment and other BACE1 exosite binders are capable to produce an allosteric modulation of the BACE1 activity. Our site-directed mutagenesis study indicated that the functional anti-BACE1 paratope, residues Tyr32 (H1), Trp50 (H2), Arg98 (H3), Phe101 (H3), Trp104 (H3) and Tyr94 (L3), strongly dominates the binding energetics with the BACE1 exosite. The mutational studies described in this work might accelerate the development of new BACE1 exosite binders with interesting pharmacological activity.

Keywords: BACE1; Alzheimer; immune complex; molecular dynamics simulation; allosteric control

1. Introduction

Alzheimer's disease (AD) is a degenerative brain syndrome first described by Alois Alzheimer in 1906 that affects more than 37 million people worldwide (Melnikova, 2007). The current "amyloid hypothesis", regarding AD treatment, correlates the increased production of amyloid beta peptides (Aβ) or reduced Aβ clearance, to the formation of Aβ deposits, leading to the progression of AD (Hardy & Selkoe, 2002; Nguyen, Yamani, & Kiso, 2006; Olson, Copeland, & Seiffert, 2001; van Marum, 2008). Aβ are generated *in vivo* through proteolysis of the amyloid precursor protein (APP) by the beta-site APP cleaving enzyme 1 (namely BACE1; EC: 3.4.23.46) a therapeutic target for AD (Crouch et al., 2008; Ghosh, Gemma, & Tang, 2008; Stockley & O'Neill, 2008; Vassar et al., 1999). BACE1 has a conserved general folding and a catalytic apparatus of the aspartic proteases superfamily and more precisely that of the pepsin subfamily (Lin et al., 2000; Sinha et al., 1999; Vassar et al., 1999; Yan et al., 1999). The crystal structures of BACE1 confirm that it contains a single polypeptide chain, while the active site is a long cleft for the substrate recognition with two catalytic aspartic residues (Hong et al., 2000, 2002). Kinetic and specificity studies showed that BACE1 interacts with approximately 11 substrate residues, showing affinity for hydrophobic residues but with a low specificity (Turner III, Hong, Koelsch, Ghosh, & Tang, 2005; Turner III et al., 2001).

In addition to the active site (Hong et al., 2000, 2002), Kornacker et al. reported the discovery of an exosite within the catalytic domain of the human BACE1 that binds small peptides in a manner that it is unaffected by the active site occupancy (Kornacker et al., 2005, 2007, 2008). Peptides that bind in this exosite are able to inhibit the ability of BACE1 to hydrolyze its natural substrate, APP. In addition, we have reported the structural and thermodynamic characteristics of this exosite (Gutierrez, Enriz, & Baldoni, 2010).

Recently, new experimental evidences showed that it is possible to inhibit the catalytic activity of BACE1 by targeting its exosite (Atwal et al., 2011; Zhou et al.,

*Corresponding author. Email: hbaldoni@unsl.edu.ar

2011). These authors have designed a bispecific monoclonal antibody (mAb) with one arm comprising a low-affinity antitransferrin Fab fragment (anti-TfR), and the other arm comprising the high-affinity anti-BACE1 Fab fragment (anti-BACE1). They showed by X-ray crystallography that these antibodies inhibit BACE1 activity by binding the BACE1 exosite. However, although X-ray crystallography can model some aspects of atomic motion, it does not provide dynamical or energetics information, which is crucial for understanding biological functions. Thus, complementary experiments, computer simulations, and modeling techniques might be used to overcome the inherently static nature of crystallographic structures in order to gain a deeper understanding of the structural and dynamical basis of the binding mode at the atomic level. Given that the antigen–antibody interaction is a conformationally specific process (Wilson & Stanfield, 1994), the work reported here is aimed to extend experimental data resulting from X-ray diffraction experiments in order to examine the Fab-BACE1 mode of binding. The characteristics and strength of the interactions involved in the Fab-BACE1 immune complex formation are exhaustively analyzed. In addition, mutational studies such as those described here might dramatically accelerate the development of new anti-BACE1 mAbs with interesting pharmacological activity.

2. Computational methods

2.1. Model preparation and simulations

The protein data bank entry 3R1G (Atwal et al., 2011) was selected as a structural template to our model. The 3R1G crystal structure contains one BACE1 molecule, one Fab heavy chain fragment (H), and one Fab light chain fragment (L) with 95 water molecules. The missing loops were built by structural superposition between our model and selected crystal coordinates by using the SuperPose program (Maiti, Van Domselaar, Zhang, & Wishart, 2004). Residues 55, 219–227, 371–372, and 448–456 in the BACE1 were built from the crystal coordinates of the 2G94 molecule (Ghosh et al., 2006), the most highly resolved complete structure of BACE1 at the time. Residues 129–133, in the Fab heavy chain fragment, were built from the crystal coordinates of the heavy chain of the 3L95 molecule (Wu, Cain-Horm, et al., 2010), which share a maximum sequence identity of 93% with the heavy chain of the 3R1G molecule, which was determined with the basic local alignment search tool (BLAST website) (Altschul et al., 1997, 2005). Due to the distance from the recognition surface and its inherent flexibility, the conformations adopted by these loops during our simulations are not influencing the binding mode. In agreement with the accepted reaction mechanism for pepsin-like enzymes (Davies, 1990; Suguna, Padlan, Smith, Carlson, & Davies, 1987), the catalytic residues, Asp32 and Asp228, were modeled in a protonated and deprotoned state, respectively. Other ionizable groups were assumed as their ionization state at pH 7.0. Missing hydrogens and/or heavy atoms, if any, were added with the Amber *LEaP* utility (Case et al., 2012) according to the residues topology database. All crystallographic water molecules were retained in our model.

All molecular dynamics simulations (MD) and subsequent structural analysis were done with the Amber12 package (Case et al., 2012). The all-atom force field ff99SB (Lindorff-Larsen et al., 2010) was used to describe the complex, whereas the water molecules were represented by the TIP3P model (Jorgensen, Chandrasekhar, Madura, Impey, & Klein, 1983). The model was solvated by creating a isometric water box, where the edges of the periodic box were at least 10 Å from the solute. Finally, the molecular system was neutralized by the adding of the proper number of counterions represented by a new tuned force field (Joung & Cheatham, 2008). To remove possible bumps, the geometry of the system went through an energy minimization process with 10,000 steps of a conjugate gradient method: (i) In the first 5000 steps, only the backbone atoms of the complex were constrained with 10 kcal/(mol Å^2) force constants. (ii) In the last 5000 steps, the solute and solvent atoms were allowed to move without any constraint. The final relaxed geometry resulted in a backbone atom root-mean-square differences in atomic positions (rmsd) lower than .5 Å from the reference crystal coordinates. Then, the system was heated in the constant volume ensemble (NVT) from 10 to 300 K in 500 ps. A Langevin thermostat (Izaguirre, Catarello, Wozniak, & Skeel, 2001) was used for temperature coupling with a collision frequency of 1.0 ps^{-1}. Hydrogen stretching motions were removed using SHAKE algorithm (Ryckaert, Ciccotti, & Berendsen, 1977) with a tolerance of 10^{-5} Å, allowing an integration time step of 2 fs. The nonbonded cut-off distance was 8.0 Å with a pair list update every 25 time steps. The particle mesh Ewald (PME) method (Essmann et al., 1995) was used to treat the long-range electrostatic interactions. The equilibration continued for 2 ns at an isothermal isobaric (NPT) ensemble (Berendsen, Postma, van Gunsteren, DiNola, & Haak, 1984) with a target pressure of 1 bar and a pressure coupling constant of 1 ps. Finally, the production was carried out at the NVT ensemble running 10 independent simulations with length limited to 20 ns, accounting for a total simulation length of .2 µs. Each individual simulation was started reading the final coordinates obtained from the equilibration phase but generating random initial velocities at the target temperature (*irest = 0, tempi = 300K*) and assigning different random seeds (*ig = −1*). The production phases were performed with the CUDA version of the pmemd executable (Goetz

et al., 2012; Grand, Goetz, & Walker, 2013). For later analysis, the coordinates of the system and energies values were saved every 5 ps.

2.2. Binding free energy calculations

The MM-GBSA protocol was applied to each MD trajectory in order to calculate the relative binding energy of the complex. Details of this method have been presented elsewhere (Kollman et al., 2000). The protocol was used within the one-trajectory approximation taking 100 equidistant snapshots from the last 10 ns of each individual trajectory and all results were averaged over 10 runs. Briefly, the binding affinity for the complex:

$$\text{anti-BACE1 Fab fragment} + \text{BACE1} \Leftrightarrow \text{Complex} \quad (1)$$

Corresponds to the free energy of association written as

$$\Delta G_{\text{binding}} = \Delta G_{\text{complex}} - (\Delta G_{\text{anti-BACE1}} + \Delta G_{\text{BACE1}}) \quad (2)$$

In the MM-GBSA protocol, the binding affinity in Equation (2) is typically calculated using

$$\Delta G_{\text{complex/anti-BACE1/BACE1}} = \Delta E_{\text{MM}} + \Delta G_{\text{solv}} - T\Delta S_{\text{solute}} \quad (3)$$

where ΔE_{MM} represents the change in molecular mechanics potential energy, ΔG_{solv} is the solvation free energy penalty, and $T\Delta S_{\text{solute}}$ is the entropic contribution to the free energy. Since entropy calculations for large systems are extremely time consuming, hardly reach a converged value, and represent a crude approximation of only the solute entropy (Kuhn & Kollman, 2000), the $T\Delta S$ term was omitted in this study.

The per residue binding energy decomposition was performed as explained elsewhere (Gohlke, Kiel, & Case, 2003). The energy contribution of each residue in the complex to the binding is given by

$$\Delta G_{\text{residue}} = \Delta E_{\text{ele}} + \Delta E_{\text{vdW}} + \Delta G_{\text{GB}} + \Delta G_{\text{SA}} \quad (4)$$

where ΔE_{ele} and ΔE_{vdW} are the differences in electrostatic and van der Waals energies, respectively. ΔG_{GB} is free energy due to the solvation process of polar contribution calculated using the generalized Born model. ΔG_{SA} is the free energy due the solvation process of nonpolar contribution and was calculated from the SASA.

The mutation-induced shift in the relative binding free energy was calculated by computational alanine scanning (CAS) method as explained elsewhere (Huo, Massova, & Kollman, 2002). The $\Delta\Delta G_{\text{CAS}}$ is calculated by comparing the alanine mutant (ΔG_{mut}) to the wild type complex (ΔG_{wt}), defined as:

$$\Delta\Delta G_{\text{CSA}} = \Delta G_{\text{mutant}} - \Delta G_{\text{wt}} \quad (5)$$

Key selected residues, except glycine and proline, from the anti-BACE1 Fab fragment interface were selected and mutated in order to evaluate such substitutions. Positive and negative values indicate unfavorable and favorable mutations, respectively. The dissociation constant K_d for the relationship described in Equation (1) is defined as $K_d = [Fab][BACE1]/[Fab\text{-}BACE1]$, where $[\ ]$ denotes the concentration of the species. Upon mutation, the change in the dissociation constant K_d in M^{-1} might be esteemed from the relation $K_d = e^{\Delta G_{\text{diss}}/RT}$, where ΔG_{diss} stands for the dissociation free energy calculated as $\Delta G_{\text{diss}} = -\Delta G_{\text{bind}}$. The ratio of the dissociation constants, $r \equiv K_d^{\text{CAS}}/K_d^{\text{wt}}$ for the wild type and the mutant complex, K_d^{wt} and K_d^{CAS}, respectively, was determined from $r = e^{\Delta\Delta G_{\text{bind}}/RT}$.

3. Results and discussion

3.1. Quality of the model system

To assess the global behavior of the simulations, certain overall structural properties were monitored over the entire trajectories. The backbone atoms rmsd were calculated and plotted for each complex component (BACE1, V_{H} and V_{L} chains, Figures S1–S3, respectively, in Supplementary data). These figures show that the rmsd reached a plateau long before the last 10 ns for each simulation. Consequently, the last 10 ns of each trajectory were considered as productive simulation time for further analyses. Table S4 shows that while the variable domains of the Fab fragment displayed no significant structural deviation (average V_{H} rmsd ~.95 Å and average V_{L} rmsd ~.75 Å), both the BACE1 and the residues located within 6 Å from the contact surface of the antigen–antibody complex have a slight deviation (rmsd ~1.61 Å and rmsd ~1.83 Å, respectively). However, this is not a major issue that might impact the system quality. In fact, the BACE1 and both V_{H} and V_{L} domains showed similar fluctuation distributions (i.e. RMSF) and similar trends of dynamic features in the 10 runs (Figures S5(a)–(c) in Supplementary data). During our dynamic simulations, the Fab elbow angle (Stanfield, Zemla, Wilson, & Rupp, 2006) passed from a crystallographic value of 128.6° to an average value of 144.5°. This value is frequently found in Fab fragments possessing a *k*L chain (Stanfield et al., 2006), and falls within the reported range of 127°–225° (Wilson & Stanfield, 1994). The above results indicate that the systems, as a whole, behaved well and that their flexibility changed to some extent. In fact, during antigen–antibody complexation, well-known ligand-induced conformational changes occur in the antigen combining site as well as in the remotest parts of the antibody (Guddat et al., 1995). Table S6 (Supplementary data) shows the mean and standard deviation

(SD) of selected energy terms averaged from the last 10 ns of simulation for each of the 10 runs. The unsigned SD is lower than the ∼.5% from its mean value, supporting the idea that all systems became energetically stable during the last half of the simulation.

In conclusion, a well-behaved simulation that achieves an adequate amount of sampling for each component of the complex (BACE1, V_H, and V_L chains) is assumed, suggesting that no significant structural drift from its starting crystallographic structure occurred.

3.2. Binding free energy contributions

As observed in Table 1, van der Waals (ΔE_{vdw}) and electrostatic (ΔE_{ele}) terms in the gas phase provide the most favorable contributions to the complex formation. In addition, the polar solvation energies (ΔG_{GB}) impair the binding, whereas the nonpolar solvation energies (ΔG_{np}) barely contribute to the Fab–BACE1 binding. Further insight into the forces involved in Fab–BACE1 complex formation might be obtained by analyzing the total electrostatics ($\Delta G_{ele,tot}$) and the total nonpolar ($\Delta G_{np,tot}$) contributions. Table 1 clearly shows that despite the favorable electrostatic energy in the gas phase (ΔE_{ele}), the contribution of the polar solvation energy to the binding (ΔG_{GB}) is unfavorable in the 10 runs. Therefore, $\Delta G_{ele,tot}$ (i.e. $\Delta E_{ele} + \Delta G_{GB}$) does not favor the binding. Table 1 also suggests that in the 10 runs, the net result of nonpolar interactions, $\Delta G_{np,tot}$ (i.e. $\Delta E_{vdw} + \Delta G_{np}$), is favorable for the complex formation. It should be noted that this behavior has been previously proposed as a general trend for noncovalent ligand–receptor associations (Miyamoto & Kollman, 1993). As demonstrated by numerous studies, the electrostatic contribution generally disfavors the binding of ligands to its receptor because the unfavorable change in the solvation electrostatics is not fully compensated by the favorable electrostatics within the resulting ligand–receptor complex (Gohlke et al., 2003; Novotny, Bruccoleri, Davis, & Sharp, 1997; Sharp, 1996). Finally, the net ΔG_{bind}, the sum of enthalpic and desolvation terms, (i.e. $\Delta G_{ele,tot} + \Delta G_{np,tot}$), remains favorable for the Fab–BACE1 complex formation in every run, covering a range from −53.66 to −80.89 kcal/mol.

In conclusion, the binding free energy obtained for this immune complex is driven by favorable nonpolar interactions rather than by the electrostatic interactions. However, long-range interactions always play an important role in the epitope–paratope binding mode (Van Oss, 1995). These results are in agreement with our previously published data, which show that the BACE1 exosite is solvent-exposed and mostly hydrophobic (Gutierrez et al., 2010; Kringelum, Nielsen, Padkjær, & Lund, 2013; Li, Huang, Swaminathan, Smith-Gill, & Mariuzza, 2005; Lijnzaad & Argos, 1997).

3.3. Free energy decomposition

3.3.1. The BACE1 epitope

According to the free energy decomposition analysis, the binding between the Fab fragment and the BACE1 exosite is driven by selected hot spots that play a major role in the Fab–BACE1 recognition. The anti-BACE1 Fab fragment binds to a quite discontinuous epitope consisting of solvent-exposed residues on the targeted BACE1 (Figure 1). These residues are located mostly within the structural elements denoted as loop C (251–258), loop D (270–273), and loop F (311–317), which are far apart in the primary sequence but assembled together by 3D folding. The contribution of an individual residue to the binding free energy varies within the range of $\Delta G = .95$ to about $-\Delta G = 3.5$ kcal/mol. Figure 1 shows that while Asp255 contributes slightly unfavorably to the binding, three residues, Lys256, Phe257 and Pro258 (located

Table 1. Energetic contributions to the binding free energy.[a]

Run	ΔE_{vdw}[b]	ΔE_{ele}[c]	ΔG_{gb}[d]	ΔG_{np}[e]	$\Delta G_{ele,tot}$[f]	$\Delta G_{np,tot}$[g]	ΔG_{bind}[h]
1	−91.70	−316.87	356.98	−14.10	40.11	−105.80	−65.69
2	−98.90	−311.96	354.43	−14.75	42.46	−113.65	−71.19
3	−93.13	−311.88	353.67	−14.40	41.79	−107.54	−65.74
4	−99.44	−258.99	316.68	−15.44	57.69	−114.88	−57.19
5	−103.09	−282.97	335.13	−15.70	52.16	−118.78	−66.63
6	−105.92	−365.27	411.62	−16.41	46.34	−122.33	−75.98
7	−91.79	−273.11	323.80	−14.34	50.69	−106.12	−55.43
8	−101.10	−272.27	324.53	−15.65	52.26	−116.75	−64.49
9	−110.60	−321.33	367.15	−16.11	45.82	−126.72	−80.89
10	−83.81	−253.89	297.00	−12.97	43.12	−96.78	−53.66
Mean[i]	−97.95	−296.85	344.10	−14.99	47.25	−112.93	−65.69
SD[i]	7.50	32.83	30.49	1.01	5.71	8.94	8.32

[a]Values are in kcal/mol and averaged over the period (10–20 ns).
[b]van der Waals, [c]electrostatic, [d]generalized Born, [e]nonpolar solvation, [f]total electrostatic, [g]total nonpolar, and [h]total free energy of binding.
[i]Averaged over the 10 runs.

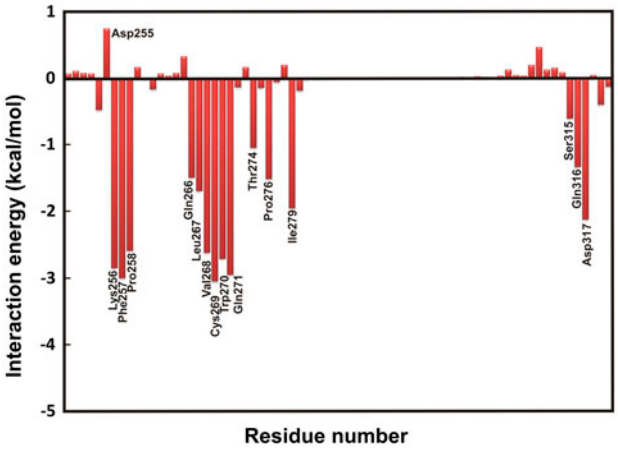

Figure 1. Antigen–antibody interaction spectrum. The *x*-axis denotes the residue number of BACE1 and the *y*-axis denotes the interaction energy contribution of individual residues.

in loop C), make significant contributions to the binding free energy, each residue providing more than $-\Delta G = 2$ kcal/mol. Only two residues located in loop D (Trp270 and Gln271) provide large contributions to the binding free energy (each residue yielding a $-\Delta G$ higher than 2 kcal/mol). However, solvent-exposed residues located downstream of loop D (the pre-amino acids sequence) make additional contributions to the binding free energy. Residues Gln266 and Leu267 contribute with a $-\Delta G$ higher than 1 kcal/mol. Residues Val268 and Cys269 also provide a favorable interaction ($-\Delta G$ over 2 kcal/mol). In addition, solvent-exposed residues located upstream of loop D (the post-amino acids sequence) (residues Thr274, Pro276, and Ile279) contribute to the binding free energy, yielding values of $-\Delta G$ higher than 1 kcal/mol. Out of the seven residues forming loop F, only Asp317 yields a $-\Delta G$ higher than 2 kcal/mol to the binding free energy; whereas residues Ser315 and Gln316 contribute to the binding, yielding a $-\Delta G$ lower than 2 kcal/mol.

The different components of the buried solvent area (BSA) (Krissinel & Henrick, 2007) upon complex formation are listed in Table S7 (Supplementary data). Our dynamics model shows a particular topography in which about 875.7 Å^2 is buried on the antigen; accounting for ~5.1% of the total accessible molecular surface of the BACE1 (17322.8 Å^2). This result is in close agreement with a previous crystallographic study (Atwal et al., 2011). Surface mapping of the buried BACE1 residues involved in the interface formation shows that 20 residues (252–254, 256–258, 266–271, 276,279, 311, 314–317, and 319) are partially buried by the V_H chain of the Fab fragment (BSA: 653.7 Å^2; ~3.8%). In turn, 11 residues on the BACE1 surface (253, 254, 256, 257, 271, 272, 274, 276, 278, 279, and 364) are partially buried by the V_L chain of the Fab fragment (BSA: 221.8 Å^2; ~1.3%).

These results clearly indicate that the BACE1 epitope is formed by structural elements noted as loops C, D, and F, and solvent-exposed residues located within about 6 Å of such loops. The residue-based decomposition analysis shows that the key residues located within the structural elements denoted as loops C and D contribute strongly to the Fab–BACE1 complex formation. These findings are in complete agreement with experimental (Atwal et al., 2011; Kornacker et al., 2007; Yu et al., 2011) and theoretical (Gutierrez et al., 2010) results aimed to locate and characterize the BACE1 exosite.

3.3.2. *The anti-BACE1 paratope*

The corresponding pair interaction energy decomposition analysis on the Fab fragment is shown in Figure 2(a) and (b). These figures are notably useful to identify the residues in the complementarity determining regions

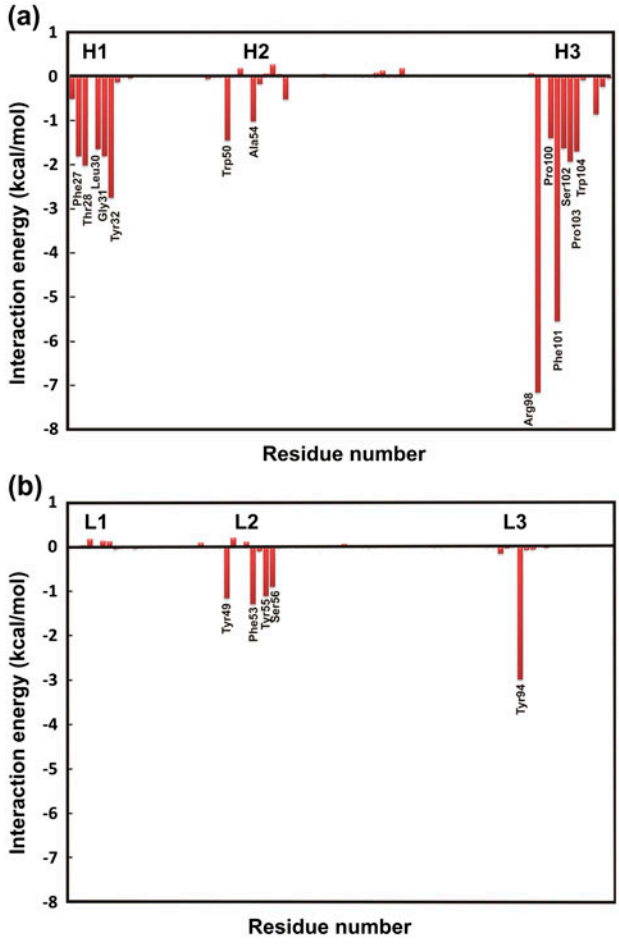

Figure 2. Antigen–antibody interaction spectrum. The *x*-axis denotes the residue number of (a) V_H and (b) V_L anti-BACE1 antibody and the *y*-axis denotes the interaction contribution energy of individual residues.

(CDRs) responsible for the BACE1 binding and its strength. Figure 2(a) and (b) clearly show that five of the six CDRs are involved in the Fab–BACE1 complex formation: H1 (H26–H32); H2 (H50–H59); H3 (H98–H107); L2 (L49–L56); and L3 (L92–L94). Residues showing large contributions ($-\Delta G$ more than 1 kcal/mol) to the binding free energy difference are: Phe27, Thr28, Leu30, Gly31, and Tyr32 (located in the H1); Trp50 and Ala54 (located in the H2); Arg98, Pro100, Phe101, Ser102, Pro103, and Trp104 (located in the H3); Tyr49, Phe53, Tyr55, and Ser56 (located in the L1); and Try94 located in the L3 loop. It is worthwhile to note that out of the 18 above-mentioned residues, only Arg98 (H3) is charged, while the rest are uncharged (nine polar and eight apolar). In addition to the above-mentioned residues, other amino acids are involved in the complex formation. However, they make a weak contribution to the binding free energy difference, providing a $-\Delta G$ value lower than 1.0 kcal/mol. On the contrary, residues located in the L1 loop do not contribute to the binding free energy difference. These results are in agreement with experimental findings showing that antigen–antibody complex formation involves interactions with residues located at the L3 loop and, in particular, the H3 loop (Padlan, Abergel, & Tipper, 1995; Persson et al., 2013). It has been reported that protein-binding antibodies have a relatively flat topography in the combining site, making noncentral loops such as L2 and H1 interact with the antigen. On the other hand, while L1 (L30–L36) contains a large number of mostly noncontacting residues, the H2 loop barely contributes to the complex formation. This finding might be explained by the gross arrangement of the CDRs with respect to the center of the combining site (i.e. H3 and L3), where most antigen interactions occur (Figure 2).

The corresponding BSA, referenced to the anti-BACE1 Fab fragment (Table S8 in Supplementary data), reveals that 847.3 Å^2 of the antibody become buried upon complex formation, accounting for about 3.6% of the total accessible molecular surface (23206.3 Å^2). The BSA of the V_H chain (616.2 Å^2; ∼2.3%) is larger than that of the V_L chain (231.1 Å^2; ∼1%). In fact, while the L1 is not buried in the complex, the BSA averages for each CDR in the Fab–BACE1 complex are: H1, 237.4 Å^2; H2, 83.6 Å^2; H3, 295.4 Å^2; L2, 133.6 Å^2, and L3, 97.4 Å^2. These values show that H1, H3, L2, and L3 are the major CDRs involved in contacting the BACE1 epitope. As expected, the preceding finding, which shows that H1, H3, L2, and L3 make a significant contribution to the contact surface of the combining site, was observed in other antibodies directed against large antigens (Collis, Brouwer, & Martin, 2003). Likewise, CDRs of the V_H chain highly contribute to the BSA than those of the V_L chain (Becker, 1996; Wilson & Stanfield, 1994).

3.4. *Epitope–paratope interactions*

The favorable contributions to the Fab–BACE1 complex formation arise from an intricate polar and apolar intermolecular interaction network between the identified epitope and paratope. Thirty-seven pairwise atomic contacts were identified (Tina, Bhadra, & Srinivasan, 2007), 14 were hydrophobic interactions, three were salt bridges, 17 were hydrogen bonds, two were cation–Pi interactions, and one was an aromatic–sulfur interaction (Tables 2 and 3). These interactions involved five of the six CRDs (H1, H2, H3, L2, L3). No intermolecular interactions were observed involving residues from the CDR L1, which was the one farthest from the BACE1 epitope and remained unburied upon complex formation. In addition, Phe27 (H1) and Trp50 (H2) were partially buried by the interaction with the BACE1 exosite (BSA of 18.0 and 16.2 Å^2, respectively) but no favorable polar and/or apolar intermolecular interactions were identified for these residues.

A good shape complementarity between the epitope–paratope interacting surface is obtained from our dynamic model (Sc ∼ .63) in agreement with the observed mean value for other antigen–antibody complexes (Lawrence & Colman, 1993). Moreover, the average interface separation was .61 Å with three water molecules. Water molecules have been previously proposed as a necessary structural requirement for overcoming imperfections in the shape complementarity characteristic of protein–antibody interactions (Mariuzza & Poljak, 1993).

3.5. *Alanine scanning mutagenesis*

In order to further elucidate the role of the key residues identified by the free energy decomposition approach, a CAS mutagenesis of selected residues located at the CDRs of the anti-BACE1 Fab fragment was carried out. The mutated residues were those that contributed with a

Table 2. Epitope–paratope hydrophobic interactions.[a]

BACE1	Fab residues
Phe257	V_H–Phe101
Pro258	
Phe261	
Val268	
Pro258	V_H–Ala54
Leu267	V_H–Leu30
Val268	V_H–Pro100
Trp270	
Trp270	V_H–Tyr32
Trp270	V_H–Pro103
Pro276	
Ile279	
Pro276	V_L–Tyr49
Phe365	V_L–Phe53

[a]within cut-off distances of <6.0 Å.

Table 3. Epitope–paratope polar interactions.[a]

Interation	BACE1	Anti-BACE1	Distance (Å)
Salt Bridge			
	Asp317–$O^{\delta1}$	V_H–Arg98–$^{\eta}{}_2{}^{H}$	2.87
	Asp317–$O^{\delta2}$	V_H–Arg98–$^{\eta}{}_1{}^{H}$	2.71
	Lys256–N^{ζ}	V_H–Asp59–$O^{\delta1}$	3.13
Hydrogen bonds			
	Glu255–N	V_L–Tyr94–OH	3.34
	Gln266–$N^{\varepsilon2}$	V_H–Leu30–O	3.36
	Gln266–$O^{\varepsilon1}$	V_H–Ala54–O	3.48
	Gln266–$N^{\varepsilon2}$	V_H–Ala54–O	3.06
	Trp270–N	V_H–Tyr32–OH	3.45
	Trp270–$N^{\varepsilon1}$	V_H–Ser102–O	2.87
	Gln316–$O^{\varepsilon1}$	V_H–Glu1–N	2.76
	Ser253–O	V_L–Tyr94–OH	2.75
	Lys256–N^{ζ}	V_H–Asp59–$O^{\delta1}$	2.95
	Gln271–$N^{\varepsilon2}$	V_L–Tyr55–OH	2.97
	Gln271$O^{\varepsilon1}$	V_L–Ser56–O^{γ}	2.96
	Ser315–O^{γ}	V_H–Thr28–$O^{\gamma1}$	3.43
	Asp317–$O^{\delta1}$	V_H–Tyr32–OH	3.08
	Asp317–$O^{\delta1}$	V_H–Arg98–NH1	2.74
	Asp317–$O^{\delta1}$	V_H–Arg98–NH2	3.45
	Asp317–$O^{\delta2}$	V_H–Arg98–NH2	2.72
	Cys269–N	V_H–Gly31–O	2.91
Cation–π			
	Lys256–N^{ζ}	V_L–Tyr94	4.61
	Lys256–N^{ζ}	V_H–Trp104	5.82
Aromatic–sulfur			
	Cys269–S^{γ}	V_H–Tyr32	5.33

[a]within cut-off distances of <6.0 Å.

$-\Delta G$ higher than 1 kcal/mol in the per residue energy decomposition (Figure 2(a) and (b)). Table 4 shows that every proposed alanine substitution significantly disrupted the binding affinity, dramatically changing some of the total binding free energy components. Affinity loss might be explained by the deletion of specific epitope–paratope interactions summarized in Tables 2 and 3.

3.5.1. *Arg98 (H3) mutation*

The highly disruptive effect of the Arg98 (H3) alanine substitution might be rationalized by the loss of a strong double salt bridge interaction (~3.2 Å; SASA ~110 Å^2) formed between $N^{\eta H}$ and $N^{\eta 1H}$ of Arg98 with $O^{\delta1}$ and $O^{\delta2}$ of Asp317 (loop F) of the BACE1 (Figure 3(a)). The mutation-induced change in binding free energy ($\Delta\Delta G_{CAS}$ ~17.0 kcal/mol) was translated to an extremely high dissociation constant (K_d ~10^{12} fold). The produced shift in the $\Delta\Delta G_{ele,tot}$ (about ~13.8 kcal/mol) correlated well with the strong salt bridge disruption.

It is worth noting that a second salt bridge (~3.8 Å) might be identified between $O^{\delta1}$ Asp59 (H2) and N^{ζ} Lys256 located at the loop C in the BACE1. However, this salt bridge is more solvent-exposed (SASA ~247 Å^2) and might be weakened by the interaction with the water molecules. This observation might explain the weak contribution of Asp59 to the per residue binding free energy difference ($-\Delta G_{bind}$ lower than .6 kcal/mol).

3.5.2. *Tyr94 (L3), Phe101 (H3), or Tyr32 (H1) mutations*

Alanine mutations of these residues increased the binding free energy from ~5.7 to ~6.9 kcal/mol, which translates to a high dissociation constant K_d from ~10^4 to ~10^5 fold, respectively. Tyr94 (L3) was involved in cation–pi interaction with Lys256 (loop C) (~5.82 and ~4.61 Å), Figure 3(b). In addition, the hydroxyl group of Tyr94 (L3) made hydrogen bonds with the main chain *N* of Glu255 (~3.3 Å) and with the main chain *O* of Ser253 (~2.7 Å), both residues located in loop C. The energy shift observed by alanine substitution of Phe101 (H3) might be rationalized by the deletion of one pi–pi stacking (~5.59 Å) with Phe257 (loop C) and three hydrophobic interactions with residues Pro258 (loop C), Phe257, and Val268 (Figure 3(c)). Affinity loss, caused by mutation of Tyr32 (H1), might be explained by the deletion of one sulfur–π interaction (~5.33 Å) which involves S^{γ} of Cys269. In addition, one hydrophobic interaction with Trp270 (loop D), and two hydrogen bonds with the main-chain N of Trp270 (loop D) and the side chain $O^{\delta1}$ of Asp317 (loop F), involved the OH of

Table 4. CAS results.[a]

Mutation	CDR	$\Delta\Delta E_{vdw}$[b]	$\Delta\Delta E_{ele}$[c]	$\Delta\Delta G_{GB}$[d]	$\Delta\Delta G_{np}$[e]	$\Delta\Delta G_{ele,tot}$[f]	$\Delta\Delta G_{np,tot}$[g]	ΔG_{Wt}[h]	ΔG_{Mut}[i]	$\Delta\Delta G_{CAS}$[j]	r[k]
S102A	H3	.98	1.59	−2.30	.08	−.71	1.05	−65.69	−65.34	.35	1.8
T28A	H1	1.29	3.05	−3.11	.19	−.06	1.47	−65.69	−64.27	1.42	10.6
L30A	H1	2.35	−.17	−.94	.20	−1.11	2.54	−65.69	−64.24	1.45	11.2
F27A	H1	.72	−.89	1.68	.00	.79	.71	−65.69	−64.17	1.52	12.6
W104A	H3	2.67	2.44	−2.03	−.11	.41	2.55	−65.69	−62.72	2.97	$\sim 10^2$
S56A	L2	.92	3.83	−4.03	2.47	−.20	3.38	−65.69	−62.45	3.24	$\sim 10^2$
F53A	L2	3.24	−.19	−1.99	2.65	−2.18	5.88	−65.69	−61.92	3.77	$\sim 10^2$
Y55A	L2	2.60	−.87	.53	2.47	−.34	5.06	−65.69	−60.92	4.77	$\sim 10^3$
Y49A	L2	3.74	1.38	−3.11	2.76	−1.74	6.49	−65.69	−60.88	4.81	$\sim 10^3$
W50A	H2	3.18	−.44	−.30	2.46	−.74	5.63	−65.69	−60.73	4.96	$\sim 10^3$
Y32A	H1	6.75	−3.63	2.49	.18	−1.14	6.92	−65.69	−59.91	5.78	$\sim 10^4$
F101A	H3	6.58	1.02	−1.79	.09	−.76	6.67	−65.69	−59.78	5.91	$\sim 10^4$
Y94A	L3	6.71	3.03	−5.95	3.15	−2.92	9.85	−65.69	−58.71	6.98	$\sim 10^5$
R98A	H3	.68	142.20	−128.40	2.51	13.80	3.18	−65.69	−48.64	17.05	$\sim 10^{12}$

[a]Values are in kcal/mol and averaged over the period (10–20 ns) from the 10 runs.
[b]van der Waals, [c]lectrostatic, [d]generalized Born, [e]nonpolar solvation, [f]total electrostatic, [g]total nonpolar, [h]wild type total free energy, [i]mutant free energy, and [j]total CAS binding results.
[k]Ratio of the dissociation constant calculated as explained in methods section.

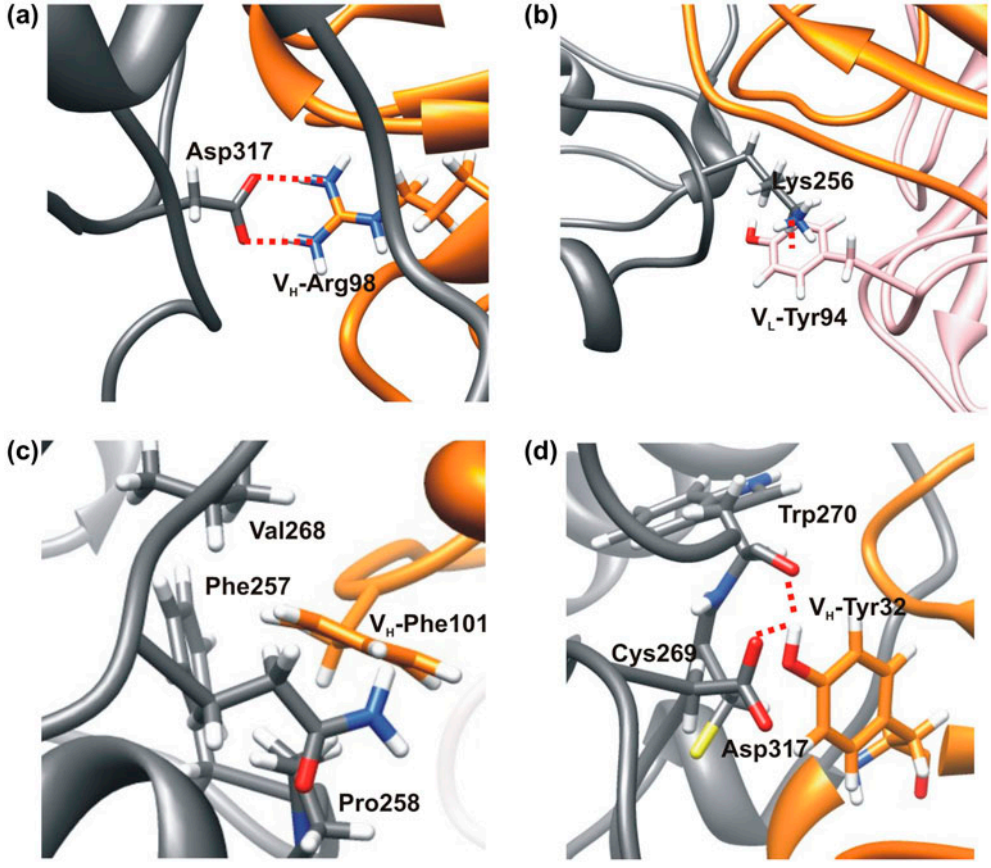

Figure 3. Important interatomic interactions located at the Fab–BACE1 interface. The interacting residues are shown in stick and labeled according the text. The BACE1 is shown in gray ribbon, while the V_H and H_L domains of the anti-BACE1 are shown in orange and pink ribbons, respectively.

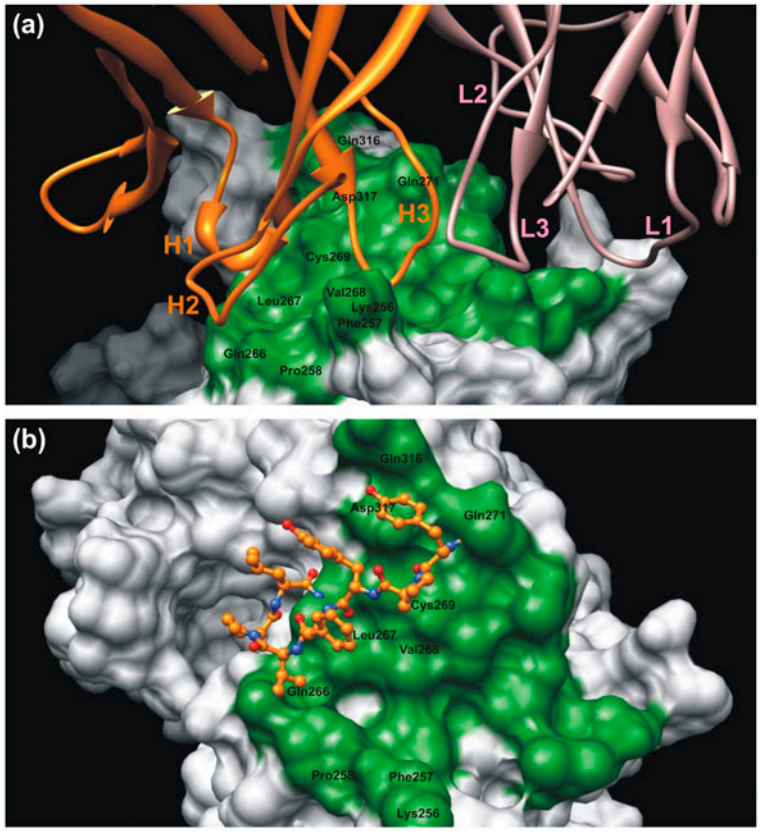

Figure 4. Surface representation of the BACE1 antibody binding region (green). The key residues of the contacting surface are labeled. (a) Mode of binding of the anti-BACE1 Fab fragment (ribbon). The heavy chain CDR loops (H1, H2, H3) are in orange, and the light chain loops (L1, L2, L3) are pink. (b) Mode of binding of a high affinity exosite binding peptide (ball and stick) (Gutierrez et al., 2010; Kornacker et al., 2005). The peptide binds along the surface sharing BACE1 hot spots with the anti-BACE1.

Tyr32 (H1) at 3.45 and 3.08 Å, respectively (Figure 3 (d)). Affinity loss might be explained by the deletion of these interatomic contacts.

3.5.3. *Tyr49 (L2), Tyr55 (L2), or Trp50 (H2) mutations*

When these residues were mutated by alanine, a significant increase in the binding free energy occurred (∼4.7 to ∼4.9 kcal/mol), compared with the wild type. These $\Delta\Delta G_{CAS}$ shifts are translated to an about $\sim 10^3$ fold change in the apparent dissociation constant due to the loss of the following interatomic forces: Tyr49 (L2) makes hydrophobic contacts with Pro276; while the OH group of Tyr55 is sc–sc hydrogen bonded (∼2.9 Å) to Glu271 $O^{\varepsilon 2}$ (loop D). No polar or apolar interactions were found for Trp50 (H2).

3.5.4. *Phe53 (L2), Ser56 (L2), or Trp104 (H3) mutations*

Alanine mutations of these residues increased the binding free energy to between ∼2.9 and ∼3.7 kcal/mol (K_d $\sim 10^2$ fold). Phe53 made hydrophobic contacts with Phe365 at the BACE1 exosite. Ser56 O^{γ} is involved in a hydrogen bond (∼2.9 Å) with Gln271 $O^{\varepsilon 1}$ (loop D); while Trp104 (H3) makes a cation–pi interaction (∼5.8 Å) with Lys256 (loop C). The loss in affinity might be well explained by the deletion of these interatomic contacts.

3.5.5. *Phe27, Thr28, or Leu30 mutations*

Alanine mutation of these residues located at the H1 loop moderately increased the apparent dissociation constant K_d (from ∼10- to ∼12 fold) due to a $\Delta\Delta G_{CAS}$ shift from ∼1.4 to ∼1.5 kcal/mol, respectively. While Phe27 is positioned in such a way that it makes no interactions with BACE1, the loss in affinity might be explained by the deletion of the following forces: residue Thr28 $O^{\gamma 1}$ is hydrogen bonded (∼3.4 Å) to Ser315 O^{γ} located in loop F; Leu30 makes hydrophobic contact with Lue267 and is main chain hydrogen bonded (∼3.3 Å) with $N^{\varepsilon 2}$ of Gln266.

3.5.6. Ser102 (H3) mutation

This mutant caused a ~1.8 fold increase in the apparent K_d by disrupting a main chain hydrogen bond (~2.8 Å) with Trp270 $N^{\varepsilon 1}$.

The CAS results show that the residues contributing the most to the Fab–BACE1 immune complex formation are located in the center (i.e. H3 and L3 loops) and in the periphery (i.e. H1 and L2 loops) of the anti-BACE Fab paratope. The strong increase in the apparent K_d (between $\sim 10^4$ and $\sim 10^{12}$ fold) caused by the alanine substitutions of Tyr32 (H1), Arg98 (H3), Phe101 (H3), and Tyr94 (L3) might allow us to define these four residues as the functional paratope of the anti-BACE1 Fab fragment. Our results are in complete agreement with experimental findings which recognize the third CDR of heavy (H3) and light chains (L3) as the most diverse and the most important loops for antigen recognition (Padlan, 1994; Zemlin et al., 2003). Finally, it is worth noting that the high propensity of Phe and Tyr to be present in the CDR has been previously reported (Birtalan et al., 2008; Wu, Sun et al., 2010). These residues are participating in the anti-BACE1 Fab fragment through their large hydrophobic effect (size), their large van der Waals interactions (polarization), their ability to form hydrogen bonds, and a restricted conformational entropy (rigidity), causing the aromatic side chains of these amino acids to be involved in strong interactions with the BACE1 epitope. In fact, it was observed that Tyr and Arg are common residues in antibody hot spots, and are often selected during somatic antibody maturation (Zemlin et al., 2003).

3.6. Biological implications

The CDRs of the anti-BACE1 and the previously published exosite binders (Gutierrez et al., 2010; Kornacker et al., 2005) bind the same exosite on the BACE1 surface although they exhibit no sequence homology. Our previous work showed that some exosite binding peptides targeted the BACE1 surface at residues Glu255–Pro258 (loop C), Gly264–Ala274 (down- and upstream of loop D), and Asp311–Tyr317 (loop F) (Gutierrez et al., 2010). Interestingly, we found in this study that the BACE1 residues (Phe257, Pro258, Val268, Cys269, Trp270, and Aps317), which contributed most energetically to bind the Fab paratope, are those residues which contacted the exosite binding peptides published elsewhere (Gutierrez et al., 2010). Considering these results, it appears that the BACE1 exosite binders recognize a steric and/or stereoelectronic surface which is similarly recognized by the H3 and L3 loops of the anti-BACE1 (Figure 4). In addition, it was previously proposed, and supported by experimental results, that the occupancy of the BACE1 exosite might affect the binding and proteolytic cleavage of large substrates probably by an allosteric mechanism (Gutierrez et al., 2010). These results are in agreement with such control mechanism because previous evidence indicates that allosterism might be at play even in the absence of changes in the receptor shape (Lee et al., 2008; Tsai, del Sol, & Nussinov, 2008). In BACE1, the neutralizing effect appears to be mediated by allosteric signal propagation, due to structural transitions, when its exosite is targeted. This assumption arises from collective dynamics analysis by low frequency modes of the BACE1 dynamics, which showed that the concerted movement of different loops (namely flap regions, 10s loop, A loop, and F loop) squeezes the substrate between the N-terminal and C-terminal lobes, initiating the catalytic activity of the BACE1 (Chakraborty, Kumar, & Basu, 2011). Furthermore, a recent report showed that the collective motions of such loops differ significantly when comparing the free and the exosite-inhibited BACE1 dynamics (Gutiérrez, Enriz, & Baldoni, 2012). The results presented here show that the strongest intermolecular interaction between the epitope–paratope involves a strong salt bridge between Arg98 (H3) and Asp317 (loop F). It should be noted that Asp317 (loop F) also plays a major role in engaging the exosite binders (Gutierrez et al., 2010; Kornacker et al., 2005). These results might explain how the anti-BACE1 Fab fragment and the exosite binders are capable of modulating the BACE1 activity.

4. Conclusions

The specificity observed for the anti-BACE1 with respect to the BACE1 exosite arises from a high shape complementarity between the interacting surfaces, the exclusion of solvent molecules, the proper positioning of the key residues, and the correct location of apolar and/or charged groups. The anti-BACE1 Fab fragment recognizes the BACE1 functional epitope located mostly within the structural elements denoted as C-loop (251–258), D-loop (270–273), and F-loop (311–317) which are far apart in the primary sequence of the BACE1, but are assembled together by 3D folding. The structural elements located up- and downstream D-loop might provide additional binding spots to the anti-BACE1 Fab fragment by providing specific intermolecular forces to the mode of binding.

Site-directed mutagenesis indicated that the functional paratope of the anti-BACE1 Fab fragment (residues Tyr32 (H1), Trp50 (H2), Arg98 (H3), Phe101 (H3), Trp104 (H3), and Tyr94 (L3)) strongly dominate the binding energetics with the BACE1 exosite. Mainly salt bridges, hydrogen bonding, and pi contacts contribute favorably to the epitope–paratope interactions. Residues located at the L2 and H1 loops might assist the epitope–paratope mode of binding by providing specific van der Waals and hydrogen bonding contacts.

These results represent an *in silico* attempt to rationalize how the BACE1 exosite binders are capable to produce an allosteric modulation of the enzymatic activity. We hope that these results might help in the understanding of the basic principles underlying the nature of the interactions with the BACE1 exosite. *In silico* mutational studies such as those described here might strongly encourage the development of new antibodies, peptides, or mimetics with interesting pharmacological activity.

Supplementary material

The supplementary material for this paper is available online at http://dx.doi.10.1080/07391102.2013.821024.

Acknowledgments

This work was supported by Universidad Nacional de San Luis (UNSL) and CONICET grants 2-0312 and PIP00474, respectively. R.D.E. and H.A.B. are staff members of the National Research Council of Argentina (CONICET, Argentina). L.J.G. gratefully acknowledges financial support from CONICET with a fellowship. We sincerely thank the anonymous reviewers for helpful comments and suggestions on the manuscript.

References

Altschul, S. F., Madden, T. L., Schäffer, A. A., Zhang, J., Zhang, Z., Miller, W., & Lipman, D. J. (1997). Gapped BLAST and PSI-BLAST: A new generation of protein database search programs. *Nucleic Acids Research, 25*, 3389–3402.

Altschul, S. F., Wootton, J. C., Gertz, E. M., Agarwala, R., Morgulis, A., Schäffer, A., & Yu, Y.-K. (2005). Protein database searches using compositionally adjusted substitution matrices. *The FEBS Journal, 272*, 5101–5109.

Atwal, J. K., Chen, Y., Chiu, C., Mortensen, D. L., Meilandt, W. J., Liu, Y., … Watts, R. J. (2011). A therapeutic antibody targeting BACE1 inhibits amyloid-β production *in vivo*. *Science Translational Medicine, 3*, 1–12.

Becker, J. C. (1996). Eradication of human hepatic and pulmonary melanoma metastases in SCID mice by antibody-interleukin 2 fusion proteins. *Proceedings of the National Academy of Sciences, 93*, 2702–2707.

Berendsen, H. J. C., Postma, J. P. M., van Gunsteren, W. F., DiNola, A., & Haak, J. R. (1984). Molecular dynamics with coupling to an external bath. *The Journal of Chemical Physics, 81*, 3684–3690.

Birtalan, S., Zhang, Y., Fellouse, F. A., Shao, L., Schaefer, G., & Sidhu, S. S. (2008). The intrinsic contributions of tyrosine, serine, glycine and arginine to the affinity and specificity of antibodies. *Journal of Molecular Biology, 377*, 1518–1528.

Case, D. A., Darden, T. A., Cheatham, T. E., Simmerling, C. L., Wang, J., Duke, R. E., …, Kollman, P. A. (2012). *Amber12*. San Francisco: University of California.

Chakraborty, S., Kumar, S., & Basu, S. (2011). Conformational transition in the substrate binding domain of *β*-secretase exploited by NMA and its implication in inhibitor recognition: BACE1-myricetin a case study. *Neurochemistry International, 58*, 914–923.

Collis, A. V., Brouwer, A. P., & Martin, A. C. (2003). Analysis of the antigen combining site: correlations between length and sequence composition of the hypervariable loops and the nature of the antigen. *Journal of Molecular Biology, 325*, 337–354.

Crouch, P. J., Harding, S.-M. E., White, A. R., Camakaris, J., Bush, A. I., & Masters, C. L. (2008). Mechanisms of A beta mediated neurodegeneration in Alzheimer's disease. *The International Journal of Biochemistry & Cell Biology, 40*, 181–198.

Davies, D. R. (1990). The structure and function of the aspartic proteinases. *Annual Review of Biophysics and Biophysical Chemistry, 19*, 189–215.

Essmann, U., Perera, L., Berkowitz, M. L., Darden, T., Lee, H., & Pedersen, L. G. (1995). A smooth particle mesh Ewald method. *Journal of Chemical Physics, 103*, 31–34.

Ghosh, A. K., Gemma, S., & Tang, J. (2008). Beta-Secretase as a therapeutic target for Alzheimer's disease. *Neurotherapeutics: The Journal of the American Society for Experimental NeuroTherapeutics, 5*, 399–408.

Ghosh, A. K., Kumaragurubaran, N., Hong, L., Lei, H., Hussain, K. A., Liu, C.-F., … Tang, J. (2006). Design, synthesis and X-ray structure of protein-ligand complexes: Important insight into selectivity of memapsin 2 (beta-secretase) inhibitors. *Journal of the American Chemical Society, 128*, 5310–5321.

Goetz, A. W., Williamson, M. J., Xu, D., Poole, D., Grand, S. L., & Walker, R. C. (2012). Routine microsecond molecular dynamics simulations with AMBER - Part I: Generalized Born. *Journal of Chemical Theory and Computation, 8*, 1542–1555.

Gohlke, H., Kiel, C., & Case, D. A. (2003). Insights into protein-protein binding by binding free energy calculation and free energy decomposition for the Ras-Raf and Ras-RalGDS complexes. *Journal of Molecular Biology, 330*, 891–913.

Grand, S. L., Goetz, A. W., & Walker, R. C. (2013). SPFP: Speed without compromise – A mixed precision model for GPU accelerated molecular dynamics simulations. *Computer Physics Communications*, *184*, 374–380.

Guddat, L., Shan, L., Fan, Z., Andersen, K., Rosauer, R., Linthicum, D., & Edmundson, A. (1995). Intramolecular signaling upon complexation. *FASEB Journal, 9*, 101–106.

Gutierrez, L. J., Enriz, R. D., & Baldoni, H. A. (2010). Structural and thermodynamic characteristics of the exosite binding pocket on the human BACE1: A molecular modeling approach. *The Journal of Physical Chemistry A, 114*, 10261–10269.

Gutiérrez, L. J., Enriz, R. D., & Baldoni, H. A. (2012). Molecular dynamics – Studies of synthetic and biological macromolecules. (L. Wang, Ed.) (pp. 151–170). InTech.

Hardy, J., & Selkoe, D. J. (2002). The amyloid hypothesis of Alzheimer's disease: Progress and problems on the road to therapeutics. *Science, 297*, 353–356.

Hong, L., Koelsch, G., Lin, X., Wu, S., Terzyan, S., Ghosh, A. K., … Tang, J. (2000). Structure of the protease domain of memapsin 2 (beta-secretase) complexed with inhibitor. *Science, 290*, 150–153.

Hong, L., Turner, R. T.III, Koelsch, G., Shin, D., Ghosh, A. K., & Tang, J. (2002). Crystal structure of memapsin 2 (beta-secretase) in complex with an inhibitor OM00-3. *Biochemistry, 41*, 10963–10967.

Huo, S., Massova, I., & Kollman, P. A. (2002). Computational alanine scanning of the 1:1 human growth hormone-receptor complex. *Journal of Computational Chemistry, 23*, 15–27.

Izaguirre, J. A., Catarello, D. P., Wozniak, J. M., & Skeel, R. D. (2001). Langevin stabilization of molecular dynamics. *The Journal of Chemical Physics, 114*, 2090–2098.

Jorgensen, W. L., Chandrasekhar, J., Madura, J. D., Impey, R. W., & Klein, M. L. (1983). Comparison of simple potential functions for simulating liquid water. *The Journal of Chemical Physics, 79*, 926–934.

Joung, I. S., & Cheatham, T. E. (2008). Determination of alkali and halide monovalent ion parameters for use in explicitly solvated biomolecular simulations. *The Journal of Physical Chemistry B, 112*, 9020–9041.

Kollman, P. A., Massova, I., Reyes, C., Kuhn, B., Huo, S., Chong, L., … Cheatham, T. E. (2000). Calculating structures and free energies of complex molecules: Combining molecular mechanics and continuum models. *Accounts of Chemical Research, 33*, 889–897.

Kornacker, M. G., Copeland, R. A., Hendrick, J. P., Lai, Z., Mapelli, C., Witmer, M. R., … Morin, P. E. (2007) US Patent No. 2007/0149763. http://www.google.com/patents/US20070149763

Kornacker, M., Copeland, R., Hendrick, J., Lai, Z., Mapelli, C., Witmer, M. R., … Riexinger, D. J. (2008). US Patent No. 7,314,726. http://www.google.com/patents/US7314726

Kornacker, M. G., Lai, Z., Witmer, M., Ma, J., Hendrick, J., Lee, V. G., … Copeland, R. (2005). An inhibitor binding pocket distinct from the catalytic active site on human beta-APP cleaving enzyme. *Biochemistry, 44*, 11567–11573.

Kringelum, J. V., Nielsen, M., Padkjær, S. B., & Lund, O. (2013). Structural analysis of B-cell epitopes in antibody: Protein complexes. *Molecular Immunology, 53*, 24–34.

Krissinel, E., & Henrick, K. (2007). Inference of macromolecular assemblies from crystalline state. *Journal of Molecular Biology, 372*, 774–797.

Kuhn, B., & Kollman, P. A. (2000). Binding of a diverse set of ligands to avidin and streptavidin: An accurate quantitative prediction of their relative affinities by a combination of molecular mechanics and continuum solvent models. *Journal of Medicinal Chemistry, 43*, 3786–3791.

Lawrence, M. C., & Colman, P. M. (1993). Shape complementarity at protein/protein interfaces. *Journal of Molecular Biology, 234*, 946–950.

Lee, J., Natarajan, M., Nashine, V. C., Socolich, M., Vo, T., Russ, W. P., … Ranganathan, R. (2008). Surface sites for engineering allosteric control in proteins. *Science, 322*, 438–442.

Li, Y., Huang, Y., Swaminathan, C. P., Smith-Gill, S. J., & Mariuzza, R. A. (2005). Magnitude of the hydrophobic effect at central versus peripheral sites in protein-protein interfaces. *Structure, 13*, 297–307.

Lijnzaad, P., & Argos, P. (1997). Hydrophobic patches on protein subunit interfaces: Characteristics and prediction. *Proteins, 28*, 333–343.

Lin, X., Koelsch, G., Wu, S., Downs, D., Dashti, A., & Tang, J. (2000). Human aspartic protease memapsin 2 cleaves the beta-secretase site of beta-amyloid precursor protein. *Proceedings of the National Academy of Sciences of the United States of America, 97*, 1456–1460.

Lindorff-Larsen, K., Piana, S., Palmo, K., Maragakis, P., Klepeis, J. L., Dror, R. O., & Shaw, D. E. (2010). Improved side-chain torsion potentials for the Amber ff99SB protein force field. *Proteins, 78*, 1950–1958.

Maiti, R., Van Domselaar, G. H., Zhang, H., & Wishart, D. S. (2004). SuperPose: A simple server for sophisticated structural superposition. *Nucleic Acids Research*, 32(Web Server issue), W590–W594.

Mariuzza, R. A., & Poljak, R. J. (1993). The basics of binding: Mechanisms of antigen recognition and mimicry by antibodies. *Current Opinion in Immunelogy, 5*, 50–55.

Melnikova, I. (2007). Therapies for Alzheimer's disease. *Nature Reviews. Drug Discovery, 6*, 341–352.

Miyamoto, S., & Kollman, P. A. (1993). What determines the strength of noncovalent association of ligands to proteins in aqueous solution? *Proceedings of the National Academy of Sciences of the United States of America, 90*, 8402–8406.

Nguyen, J. T., Yamani, A., & Kiso, Y. (2006). Views on amyloid hypothesis and secretase inhibitors for treating Alzheimer's disease: Progress and problems. *Current Pharmaceutical Design, 12*, 4295–4312.

Novotny, J., Bruccoleri, R. E., Davis, M., & Sharp, K. A. (1997). Empirical free energy calculations: A blind test and further improvements to the method. *Journal of Molecular Biology, 268*, 401–411.

Olson, R. E., Copeland, R. A., & Seiffert, D. (2001). Progress towards testing the amyloid hypothesis: Inhibitors of APP processing. *Current Opinion in Drug Discovery & Development, 4*, 390–401.

Padlan, E. A. (1994). Anatomy of the antibody molecule. *Molecular Immunelogy, 31*, 169–217.

Padlan, E. A., Abergel, C., & Tipper, J. P. (1995). Identification of specificity-determining residues in antibodies. *The FEBS Journal, 9*, 133–139.

Persson, H., Ye, W., Wernimont, A., Adams, J. J., Koide, A., Koide, S., Lam, R., & Sidhu, S. S. (2013). CDR-H3 diversity is not required for antigen recognition by synthetic antibodies. *Journal of Molecular Biology, 425*, 803–811.

Ryckaert, J., Ciccotti, G., & Berendsen, H. J. C. (1977). Numerical integration of the cartesian equations of motion of a system with constraints: molecular dynamics of n-alkanes. *Journal of Computational Physics, 341*, 321–341.

Sharp, K. A. (1996). Electrostatic interactions in hirudin-thrombin binding. *Biophysical Chemistry, 61*, 37–49.

Sinha, S., Anderson, J. P., Barbour, R., Basi, G. S., Caccavello, R., Davis, D., … John, V. (1999). Purification and cloning of amyloid precursor protein beta-secretase from human brain. *Nature, 402*, 537–540.

Stanfield, R. L., Zemla, A., Wilson, I. A., & Rupp, B. (2006). Antibody elbow angles are influenced by their light chain class. *Journal of Molecular Biology, 357*, 1566–1574.

Stockley, J. H., & O'Neill, C. (2008). Understanding BACE1: Essential protease for amyloid-beta production in Alzheimer's disease. *Cellular and Molecular Life Sciences: CMLS, 65*, 3265–3289.

Suguna, K., Padlan, E. A., Smith, C. W., Carlson, W. D., & Davies, D. R. (1987). Binding of a reduced peptide inhibitor to the aspartic proteinase from Rhizopus chinensis: Implications for a mechanism of action. *Proceedings of the National Academy of Sciences of the United States of America, 84*, 7009–7013.

Tina, K. G., Bhadra, R., & Srinivasan, N. (2007). PIC: Protein Interactions Calculator. *Nucleic Acids Research, 35*, 473–476.

Tsai, C. J., del Sol, A., & Nussinov, R. (2008). Allostery: Absence of a change in shape does not imply that allostery is not at play. *Journal of Molecular Biology, 378*, 1–11.

Turner, R. T.III, Hong, L., Koelsch, G., Ghosh, A. K., & Tang, J. (2005). Structural locations and functional roles of new subsites S5, S6, and S7 in memapsin 2 (beta-secretase). *Biochemistry, 44*, 105–112.

Turner, R. T. III, Koelsch, G., Hong, L., Castanheira, P., Ermolieff, J., Ghosh, A. K., … Ghosh, A. (2001). Subsite specificity of memapsin 2 (beta-secretase): Implications for inhibitor design. *Biochemistry, 40*, 10001–10006.

van Marum, R. J. (2008). Current and future therapy in Alzheimer's disease. *Fundamental & Clinical Pharmacology, 22*, 265–274.

Van Oss, C. J. (1995). Hydrophobic, hydrophilic and other interactions in epitope-paratope binding. *Molecular Immunelogy, 32*, 199–211.

Vassar, R., Bennett, B. D., Babu-Khan, S., Kahn, S., Mendiaz, E. A., Denis, P., … Citron, M. (1999). Beta-secretase cleavage of Alzheimer's amyloid precursor protein by the transmembrane aspartic protease BACE. *Science, 286*, 735–741.

Wilson, I. A., & Stanfield, R. L. (1994). Antibody-antigen interactions: New structures and new conformational changes. *Current Opinion in Structural Biology, 4*, 857–867.

Wu, D., Sun, J., Xu, T., Wang, S., Li, G., Li, Y., & Cao, Z. (2010). Stacking and energetic contribution of aromatic islands at the binding interface of antibody proteins. *Immuneme Research, 6*, S1.

Wu, Y., Cain-Hom, C., Choy, L., Hagenbeek, T. J., de Leon, G. P., Chen, Y., … Siebel, C. W. (2010). Therapeutic antibody targeting of individual Notch receptors. *Nature, 464*, 1052–1057.

Yan, R., Bienkowski, M. J., Shuck, M. E., Miao, H., Tory, M. C., Pauley, A. M., … Gurney, M. E. (1999). Membrane-anchored aspartyl protease with Alzheimer's disease beta-secretase activity. *Nature, 402*, 533–537.

Yu, Y. J., Zhang, Y., Kenrick, M., Hoyte, K., Luk, W., Lu, Y., … Dennis, M. S. (2011). Boosting brain uptake of a therapeutic antibody by reducing its affinity for a transcytosis target. *Science Translational Medicine, 3,* 84ra44.

Zemlin, M., Klinger, M., Link, J., Zemlin, C., Bauer, K., Engler, J. A., … Kirkham, P. M. (2003). Expressed murine and human CDR-H3 intervals of equal length exhibit distinct repertoires that differ in their amino acid composition and predicted range of structures. *Journal of Molecular Biology, 334*, 733–749.

Zhou, L., Chávez-Gutiérrez, L., Bockstael, K., Sannerud, R., Annaert, W., May, P. C., … De Strooper, B. (2011). Inhibition of beta-secretase *in vivo* via antibody binding to unique loops (D and F) of BACE1. *The Journal of Biological Chemistry, 286*, 8677–8687.